

Microscopic Analysis of Low-Frequency Flux Noise in $\text{YBa}_2\text{Cu}_3\text{O}_{7-x}$ Direct Current Superconducting Quantum Interference Devices

D. Doenitz, R. Straub, R. Kleiner, D. Koelle

Universität Tübingen, Physikalisches Institut { Experimentalphysik II, D-72076 Tübingen, Germany

We use low-temperature scanning electron microscopy combined with SQUID detection of magnetic flux to image vortices and to investigate low-frequency flux noise in $\text{YBa}_2\text{Cu}_3\text{O}_{7-x}$ thin film SQUIDs. The low-frequency flux noise shows a nonlinear increase with magnetic cooling field up to 60 T. This effect is explained by the surface potential barrier at the SQUID hole. By correlating flux noise data with the spatial distribution of vortices, we obtain information on spatial fluctuations of vortices on a microscopic scale, e.g. an average vortex hopping length of approximately 10 nm.

PACS numbers: 68.37.Hk, 74.40.+k, 74.60.Ge, 74.76.Bz, 85.25.Dg

The sensitivity of superconducting quantum interference devices (SQUIDs) based on high transition temperature T_c superconductors is in most cases limited by low-frequency flux noise, with the spectral density of magnetic flux noise S_Φ typically scaling as $S_\Phi / 1/f$ [1, 2]. The main source of this excess noise is the thermally activated vortex motion in the high- T_c thin films forming the body of the SQUID or the superconducting input circuit [2]. Low-frequency fluctuations induced by hopping of vortices are strongly dependent on the nature and spatial distribution of defects which act as pinning sites for vortices. Therefore, integral measurements of flux noise and electric transport properties give only very limited information on the underlying vortex dynamics. Hence, techniques offering spatial information are very useful to obtain a better understanding of the basic mechanisms of low-frequency flux noise generation.

Over the last two decades, low-temperature scanning electron microscopy (LT SEM) has proven to be very successful in getting local information on properties of superconducting thin films and Josephson junctions, such as the spatial distribution of critical temperature T_c or critical current density j_c and of Josephson vortices in long junctions [3]. Recently, this method was successfully extended to the direct imaging of vortices in $\text{YBa}_2\text{Cu}_3\text{O}_{7-x}$ (YBCO) SQUIDs [4]. Together with a simultaneous measurement of the low-frequency flux noise of the SQUID, one obtains both images of the spatial distribution of vortices and local information on noise properties of the devices under investigation [5].

In this paper we investigate YBCO dc SQUIDs by LT-SEM to study the increase of magnetic flux noise with magnetic cooling field and to analyze the mechanism of low-frequency flux noise generation on a microscopic scale.

In our experiments, we use epitaxially grown YBCO thin film dc SQUIDs of the so-called washer design [see Fig. 1(a)]. The c-axis oriented YBCO film has a thickness of 80 nm; the washer size is $120 \times 305 \text{ } \mu\text{m}^2$, with a 100 μm long and 4 μm wide slit. The 1 μm wide Josephson junctions are formed by a 24 μm metric grain boundary in the underlying SrTiO_3 substrate. The YBCO SQUIDs are mounted on a magnetically shielded, liquid nitrogen cooled cryostage of a SEM [7] and read out by a standard flux-locked loop (FLL) with 3.125 kHz bias current reversal to eliminate $1/f$ noise due to fluctuations in the critical current I_c of the Josephson junctions.

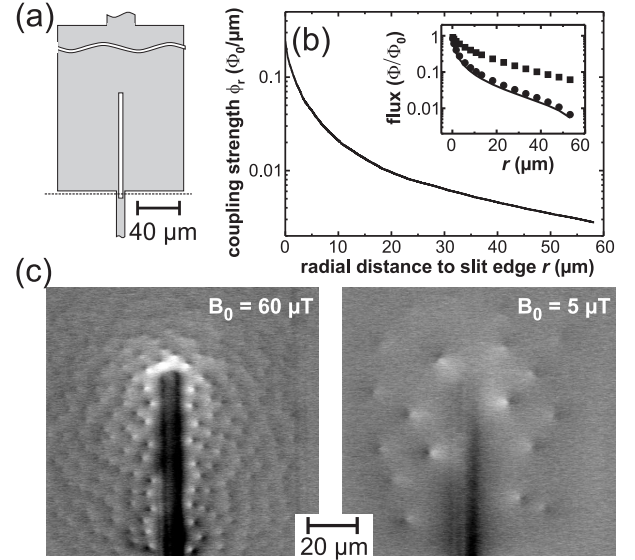


FIG. 1: (a) SQUID washer design; dotted line indicates grain boundary. (b) Coupling strength Φ_r vs. radial distance r from the slit [numerical calculation for design in (a)]. Inset: Magnetic flux $\Phi = \Phi_0(r)$ coupled by a single vortex into the SQUID hole; numerical calculation for design in (a) [squares] and for a circular washer [disks]; the line is obtained from analytical calculation [6] for a circular washer. (c) Images of the SQUID washer for two different cooling fields B_0 ($T = 77 \text{ K}$).

For the spatially resolved measurements, the electron beam is used as a local perturbation which induces an increase in temperature $T(x_0, y_0)$ on the sample surface (in the x - y -plane) centered around the beam spot position (x_0, y_0) . The length scale for the spatial decay of the thermal perturbation is set by the beam-electron range $R \approx 0.5 \text{ } \mu\text{m}$ for a typical beam voltage $V_b = 10 \text{ kV}$ [3]. This gives a maximum increase in beam induced temperature $T \approx 1 \text{ K}$ at (x_0, y_0) for a typical beam current $I_b = 7 \text{ nA}$. So-called (x_0, y_0) images are obtained by recording the e-beam induced flux change in the SQUID as a function of the e-beam coordinates (x_0, y_0) . To improve the signal to noise ratio, we use a beam-blanking unit operating at typically 5 kHz and the output signal of the FLL, i.e., the e-beam induced flux change in the SQUID, is lock-in detected. Additionally,

the time trace or the power spectrum of the FLL output signal can be recorded by a signal analyzer.

The mechanism of imaging of vortices is explained in Ref. [4] and can be briefly described as follows: The e-beam-induced local increase in temperature induces a local increase in the London penetration depth λ_L . Hence, the screening currents circulating around a vortex are spatially extended due to e-beam irradiation. If the e-beam is scanned across a vortex this vortex is virtually dragged along with the beam, i.e., it is displaced by some distance r , if the beam spot is within the radial distance R from the vortex. This displacement changes the amount of stray magnetic flux that a vortex couples to the SQUID hole. Hence, scanning across a vortex induces a negative (positive) flux change in the SQUID if the vortex is moved away from (towards) the SQUID hole. Figure 1(c) shows two examples of images with vortices appearing as pairs of positive (bright) and negative (dark) signals. These images were taken after cooling from above T_c to $T = 77$ K in a static magnetic field $B_0 = 60$ T and 5 T. The maximum displacement r of a vortex is of the order of the beam-induced change in λ_L (typically 20 nm in our experiments at 77 K) [5]. The displacement r induces a signal $\Phi = \frac{\partial \Phi}{\partial r}(r) r$, with r being the radial distance of the vortex from the SQUID hole.

For a given washer geometry, the coupling strength $r(r) = \frac{\partial \Phi}{\partial r}(r)$ is a function of the vortex position only. Therefore, it can only be obtained from a spatially resolved measurement. r plays an important role for the signal noise as well: The flux noise S_i from a moving vortex is $S_i = \frac{2}{r}(r_i) S_{ri}$, where S_{ri} is the spectral density of radial motion of the vortex at distance r_i [5].

By numerical simulation [8] one can calculate the amount of stray flux that a single vortex couples into the SQUID hole. For a given SQUID design, this value to a good approximation depends for vortices to the left or right of the SQUID hole [see Fig. 1(a)] only on the distance r from the SQUID hole. The dependence $r(r)$ (normalized to the flux quantum Φ_0) is shown in the inset of Fig. 1(b). We note that analytical calculations of $r(r)$ for circular washers [6] are in excellent agreement with our numerical simulation results [c.f. inset of Fig. 1(b)]. We find that $r(r)$ strongly depends on the washer geometry; e.g. $r(r)$ falls off with increasing r much more rapidly for a circular washer as compared to a square washer. Generally, $r(r)$ quickly falls off from $r_0(r=0)$ with increasing r and approaches zero at the outer washer edge. The derivative of this function, the coupling strength $r(r)$, shows a similar behavior [see Fig. 1(b)]. This has two important effects on vortices located close to the SQUID hole: On the one hand, the signal contrast in the image is high, since $\Phi \propto r$. On the other hand, the noise signal produced by them ally activated motion of the vortex contributes strongly to the total noise, since $S \propto \frac{2}{r}$.

Vortices in superconducting thin films show them ally activated hopping between two (or more) pinning sites. Due to the small hopping length, the hopping process cannot be resolved directly by LT SEM, but it appears as a random telegraph signal (RTS) in the SQUID response due to a change in the magnetic flux coupled to the SQUID hole. Sometimes, the SQUID signal is dominated

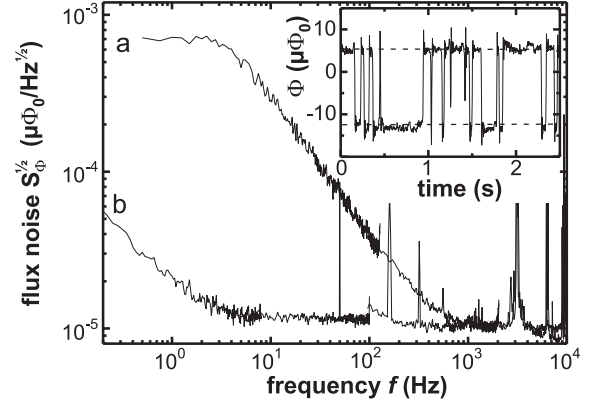


FIG. 2: Rms flux noise of YBCO dc SQUID at 77 K showing Lorentzian noise due to a single dominating actuator (a) and low-frequency $1/f$ -noise (b). Inset: time trace of the SQUID output with a single dominating actuator.

by a single actuator. In this case the RTS is clearly visible [see inset in Fig. 2], producing a Lorentzian-shaped noise spectrum [9] [see trace (a) in Fig. 2]. An uncorrelated superposition of many RTSs leads to a $1/f$ -shaped noise spectrum, provided the energies of the potential barriers between the pinning sites are distributed uniformly [10] [see trace (b) in Fig. 2].

For uncorrelated fluctuations of N vortices trapped in the washer, the total noise is

$$S = \sum_{i=1}^N \frac{2}{r}(r_i) S_{ri} = \overline{S_r} K$$

where $\overline{S_r}$ is the average spectral displacement noise power and $K = \sum_{i=1}^N \frac{2}{r}(r_i)$ is the sum of the squared coupling strengths. With the vortex positions r_i , obtained from the images (for different B_0 , i.e. different N) and the calculated function $r(r)$ we determine $K(N)$ [see Fig. 3]. Surprisingly, we find $K \propto N^{1.5}$ instead of $K^{\text{hom}} \propto N$, which is expected for a homogeneous distribution of vortices, and which we calculate by replacing the sum with the integral $N \int \frac{2}{r}(r) dr$. Furthermore, we find $K^{\text{hom}} > K$ for all N [see dashed line in Fig. 3].

The reason for this deviation is a superproportional increase of the density of vortices close to the SQUID hole with increasing B_0 , as imaged by LT SEM [see inset of Fig. 3]. This result can be explained by the formation of a surface barrier for vortex exit at the washer edges: For low magnetic fields, i.e. few vortices in the washer structure, the vortices are far apart from each other. In this case the repulsive surface barrier potential [11] is large compared to the repulsive vortex-vortex interaction [12], preventing formation of vortices close to the SQUID hole during the cooling process. For higher fields, i.e. increased vortex density, the vortex-vortex repulsion becomes stronger, thus pushing vortices closer to the SQUID hole.

With $S \propto K$ and the scaling $K \propto N^{1.5}$ shown in Fig. 3, one expects S to increase stronger than linear with the number of vortices N or magnetic field. Figure

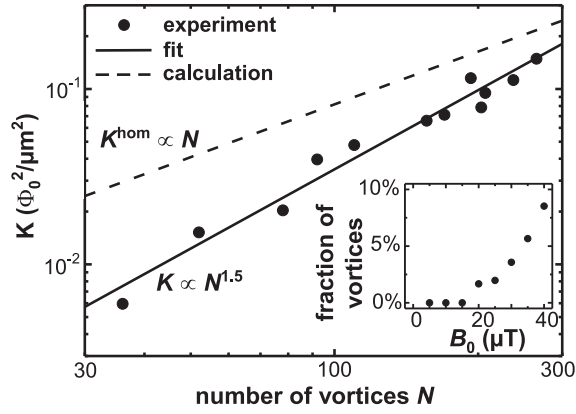


FIG. 3: Sum of squared coupling strengths K vs. number of vortices N . Dashed line: homogeneous vortex distribution. Inset: fraction of vortices found at a distance δ m from the slit edge for different cooling fields B_0 .

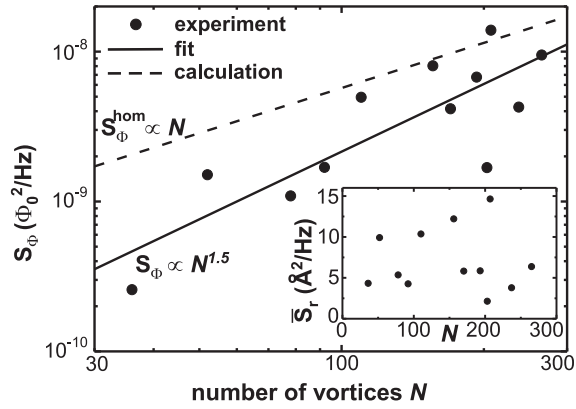


FIG. 4: Spectral density of flux noise S (1 Hz) vs. number of vortices N . Dashed line: homogeneous vortex distribution. Inset: Average spectral density of radial motion S_r (1 Hz) vs. N , calculated from K and S (1 Hz).

4 shows data for S (1 Hz) vs. N . Although $S(N)$ scatters quite strongly, it can be clearly seen that it increases more like $\propto N^{1.5}$ than $\propto N$, in contrast to previous measurements on larger SQUID washers[1]. By measuring

S (1 Hz) and determining K from the pictures, one can calculate $\overline{S_r}$ (1 Hz) using $S = \overline{S_r} K$ [see inset of Fig. 4]. $\overline{S_r}$ (1 Hz) is found to be 0.2-1.5 nm²/Hz. For a homogeneous vortex distribution, assuming $\overline{S_r} = 0.7$ nm²/Hz, one would get S^{hom}/N with $S^{\text{hom}} > S$ in the investigated field range [see dashed line in Fig. 4].

From these data it is possible to estimate the average vortex hopping length $\overline{x_r}$ using a model based on the following assumptions: (i) All vortices are situated in a symmetric double well potential with fixed distance $\overline{x_r}$ of local minima and variable barrier energy E . (ii) The barrier energies E are distributed uniformly, such that the highest (lowest) characteristic frequency f_c [10] is 1000 Hz (0.01 Hz). This condition provides an $1/f$ -shaped spectrum. Now $\overline{x_r}$ can be calculated using the flux noise theory developed in Refs. [10] and [1]. The result is $\overline{x_r} = (3 \pm 8)$ nm. This calculation gives the hopping length in radial direction. Considering hopping in two dimensions, these numbers have to be multiplied by the factor $\sqrt{2}$ to obtain the overall average hopping length $\overline{x} = (5 \pm 13)$ nm. Although this model uses some rather simple approximations it should produce the correct order of magnitude of the vortex hopping length.

In conclusion, we combined vortex imaging by LT SEM with measurements of low-frequency flux noise in YBCO dc SQUIDs to obtain information on spatial fluctuations of vortices on a microscopic scale. We have shown that a nonlinear increase of the flux noise with magnetic cooling field can be explained by a surface barrier effect. Our results clearly show that either strong pinning or avoiding of vortices trapped close to the SQUID hole is essential for reducing low-frequency flux noise. Furthermore, our analysis yields an average vortex hopping length around 10 nm for our films. The nature of defects producing pinning sites with hopping lengths on this scale still has to be revealed.

We thank K. Barthel for fabricating the YBCO SQUIDs and John Clarke for providing detailed layouts of the Berkeley SQUID readout electronics. Furthermore, we gratefully acknowledge helpful discussions with E.H. Brandt, T. Dahm, E. Goldobin, C. Iniotakis and with R. Humphreys who also kindly provided unpublished results. This work was supported by the Deutsche Forschungsgemeinschaft, the Evangelisches Studienwerk e.V. Villigst and the ESF program VORTEX.

[1] M. J. Ferrari, M. Johnson, F. Wellstood, J. Kingston, T. Shaw, and J. Clarke, J. Low Temp. Phys. 94, 15 (1994).
 [2] D. Koelle, R. Kleiner, F. Ludwig, E. Dantsker, and J. Clarke, Rev. Mod. Phys. 71, 631 (1999).
 [3] R. Gross and D. Koelle, Rep. Prog. Phys. 57, 651 (1994).
 [4] D. Koelle, R. Gross, R. Straub, S. Keil, M. Fischer, M. Peschka, R. P. Huebener, and K. Barthel, Physica C 332, 148 (2000).
 [5] R. Straub, S. Keil, R. Kleiner, and D. Koelle, Appl. Phys. Lett. 78, 3645 (2001).
 [6] R. Humphreys, IEEE Trans. Appl. Supercond. 9, 3741

(1999).
 [7] R. Gerber, T. Nissel, H.-G. Werner, A. Wilhelmann, R. Huebener, D. Koelle, and R. Gross, Cryogenics 37, 21 (1997).
 [8] M. Khabaev, M. Kupriyanov, E. Goldobin, and M. Siegel, Supercond. Sci. Tech. 16, 24 (2003).
 [9] S. Machlup, J. App. Phys. 25 (3), 341 (1954).
 [10] P. Dutta, P. Dimon, and P. Hom, Phys. Rev. Lett. 43 (9), 646 (1979).
 [11] E. Brandt, Rep. Prog. Phys. 58, 1465 (1995).
 [12] J. Pearl, Appl. Phys. Lett. 5, 65 (1964).